

IDENTIFICATION OF SHEET METAL PLASTIC ANISOTROPY, AND OPTIMIZATION OF INITIAL BLANK SHAPE IN DEEP DRAWING

Monica Iordache¹, Mihaela Teaca^{1,2}, Isabelle Charpentier²,
Marion Martiny², Gérard Ferron²

¹Facultatea de Mecanica si Tehnologie, Universitatea din Pitesti, Romania

²Laboratoire de Physique et Mécanique des Matériaux,

Université Paul Verlaine-Metz, France

email : iordache_md@yahoo.com

ABSTRACT

The present paper first aims of identifying the anisotropic plastic behavior of metal sheets by combining the results of classical uniaxial tensile tests and of heterogeneous biaxial tensile tests on cruciform specimens. The analysis was performed for both steel sheets and aluminum alloy sheets. Then, the material parameters are used in finite element simulations to predict the formation of ears in the cup drawing test. Very good predictions of experimentally-measured ears are obtained for all materials. Finally, a correction of the initial contour is proposed, which allows us to prevent the formation of ears at the end of the drawing process.

KEYWORDS: Sheet metals, anisotropy, deep-drawing, finite element method.

1. INTRODUCTION

Sheet metals obtained by cold-rolling exhibit a crystallographic texture resulting from the elaboration process. Therefore, the mechanical behavior of these materials is anisotropic, with 3 orthogonal planes of symmetry defined by the rolling direction, the transverse direction and the thickness direction. In particular, plastic anisotropy plays a major role in the forming processes that are used to transform flat sheets in complex parts, for instance in the automotive components, or in domestic appliances. The parameter commonly used to characterize this behavior is the anisotropy coefficient, or Lankford coefficient R , defined in uniaxial tensile tests on rectangular sheet specimens by :

$$R = \frac{\varepsilon_2}{\varepsilon_3} \quad (1)$$

where ε_2 and ε_3 are the plastic strains along the width direction and the thickness direction of the specimen, respectively. In the general case of transverse anisotropy, this coefficient depends on the angle α between the rolling direction and the tensile axis. Material anisotropy is usually characterized by determining the three values R_0 , R_{45} and R_{90} ,

obtained in uniaxial tension along the rolling direction (RD), the diagonal direction (DD) and the transverse direction (TD), inclined at 0° , 45° and 90° from the rolling direction, respectively.

The Lankford coefficient $R(\alpha)$ is a measure of *strain*-anisotropy. However, plastic anisotropy also manifests by *stress*-anisotropy, i.e., by variations of the uniaxial yield stress $\sigma(\alpha)$.

The effect of plastic anisotropy is clearly apparent in the deep-drawing test of cylindrical cups. In this test, the formability can be characterized by the Limiting Drawing Ratio (LDR), which is the largest value of the ratio between initial blank diameter and punch diameter that can be successfully reached, without necking and failure of the cup. The LDR is an increasing function of the average R -value.

Another effect of plastic anisotropy is the formation of ears and troughs around the cup [1-3]. This effect has received two different explanations, both of them based on the observation that an element of the contour situated at the angle α from RD is submitted to a uniaxial compression in the orthoradial direction, defined by the angle $\beta = \alpha + \pi/2$ from RD. The first explanation [4] considers that a higher elongation in the radial direction and a lower thickening are obtained with a higher value of the

Lankford coefficient $R(\beta)$. Thus, the formation of a ear is expected to be associated with a maximum of $R(\beta)$. The second explanation [5] considers that the shape of the contour is imposed by the shear-strain obtained in uniaxial tension/compression at the angle β , which can be quantified by the coefficient $\Gamma(\beta) = \dot{\epsilon}_{\alpha\beta} / \dot{\epsilon}_{\beta\beta}$, where $\dot{\epsilon}_{\alpha\beta}$ and $\dot{\epsilon}_{\beta\beta}$ are the shear and normal strain-rate components, respectively. The coefficient $\Gamma(\beta)$ is linked to the angular evolution of the uniaxial yield stress $\sigma(\beta)$ by:

$$\Gamma(\beta) = -\frac{\partial\sigma(\beta)/\partial\beta}{2\sigma(\beta)} \quad (2)$$

Thus, the formation of a ear is expected to be associated with a minimum of $\sigma(\beta)$. The two explanations lead to the same qualitative predictions in a number of situations, for instance, in steels where a minimum of $R(\alpha)$ is observed together with a maximum of $\sigma(\alpha)$ for $0 \leq \alpha \leq \pi/2$. In this case, ears form along RD and TD. However, a quantitative assessment of the height of ears is not so clear. In particular, the height of ears predicted in numerical simulations strongly depends on the plasticity model employed, when the model parameters are determined in order to fit given values of R_0 , R_{45} and R_{90} [2,3]. This observation suggests that the evolution of $\sigma(\alpha)$ should also be taken into account in the identification of a model giving a proper account of material anisotropy.

In this paper, the anisotropy parameters defining the shape of the yield surface are identified by means of classical uniaxial tensile tests and of heterogeneous biaxial tensile tests on cruciform specimens. Then, the earing profiles predicted by numerical simulations on initially circular blanks are compared with experimental ones. Finally, a modification of the initial contour is proposed, in order to obtain ear-free cups.

2. EXPERIMENTAL PROCEDURE

In the uniaxial and biaxial tensile tests, the strains at the surface of the specimens were measured using an image correlation technique.

The uniaxial tensile tests were performed on a conventional Zwick tension-compression machine, on specimens cut along RD, DD and TD. The Lankford coefficient R was then calculated by using the surface strains obtained with the image correlation technique, and by taking account of the contribution of elastic strains and of the assumption of plastic incompressibility.

The biaxial tensile tests were performed using a specific device developed by Ferron and Makinde [6]. The device consists of a spatial-arm mechanism which can be mounted on a conventional tension-compression machine and tested in compression to generate an equibiaxial stretching state on a cruciform specimen, fig. 1.

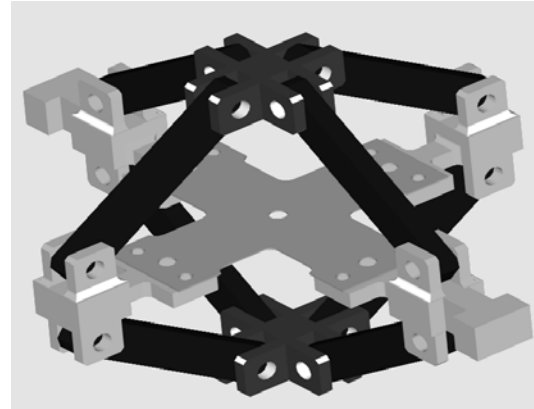
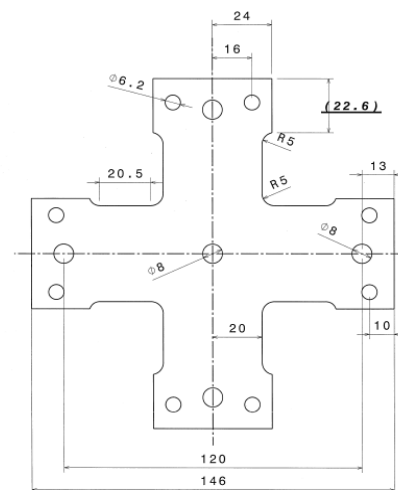
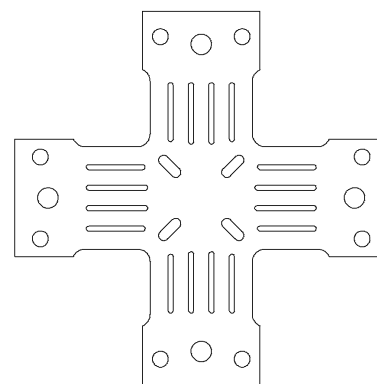


Fig. 1 Schematic view of the experimental device



(a) UT/PST specimen



(b) UT/EBT specimen

Fig. 2 Biaxial tensile specimens

Two types of specimens were designed, with the aim of offering a high sensitivity of the strain fields obtained under biaxial stretching to plastic anisotropy. The stress range goes from uniaxial tension (UT) to plane-strain tension (PST) for the first type of specimen (UT/PST specimen, fig. 2a), and from uniaxial tension to equibiaxial tension (EBT) for the second type (UT/EBT specimen, fig. 2b).

A number of preliminary simulations have been performed to analyze the sensitivity of strain fields obtained on biaxial specimens to material anisotropy. The first-order physical quantities that control the strain fields in UT/PST and UT/EBT specimens are the stress-ratios σ_{ps}/σ_u and σ_b/σ_u , respectively, where σ_u, σ_{ps} and σ_b are the yield stresses in uniaxial, plane-strain and equibiaxial tension, respectively.

3. MATERIAL MODELLING AND IDENTIFICATION STRATEGY

Since the earlier anisotropic yield criterion proposed by Hill [7], anisotropic yield functions of increasing complexity have been developed during the last 30 years [8-13]. The yield function proposed in [11], called FMM model in the following, is considered here for material parameters identification. It includes 8 parameters (6 reals and 2 integers) for defining the adimensional yield surface.

The FMM model was originally expressed under the assumption of plane-stress conditions. The yield surface is defined in principal stress plane (σ_1, σ_2) using the polar-coordinate representation described by the function $g(\theta, \alpha)$, where g is the radius to a point of the yield surface, θ is the polar angle on the yield surface, and α is the angle between orthotropic axes and principal stress axes. The principle of this description is presented on fig. 3, where the yield surfaces are normalized by the effective stress $\bar{\sigma}$, and are drawn for different α -values.

The function $g(\theta)$ for transversely isotropic (normally anisotropic) materials is expressed as :

$$(1 - k)g(\theta)^{-6} = F(\theta) = (\cos^2 \theta + A \sin^2 \theta)^3 - k \cos^2 \theta (\cos^2 \theta - B \sin^2 \theta)^2 \quad (3)$$

and its extension to transverse anisotropy is defined by:

$$(1 - k)^{m/6} g(\theta, \alpha)^{-m} = F(\theta)^{m/6} - 2a \sin \theta \cos^{2n-1} \theta \cos 2\alpha + b \sin^{2p} \theta \cos^2 2\alpha \quad (4)$$

where k, A, B, a, b and m are real numbers, and exponents n and p are positive integers.

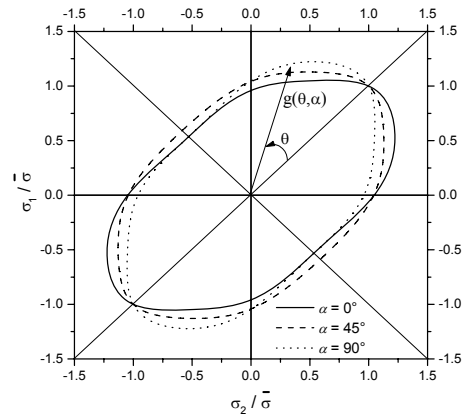


Fig. 3 Sketch of the yield surface in principal stress space (σ_1, σ_2) , for different values of angle α between rolling direction and principal stress axis s_1

The 3D-extension of the criterion presented in [14] is used in numerical simulations, which are performed using the Abaqus/Explicit finite element code with the VUMAT subroutine.

An interesting property of the FMM yield function is that, for given values of the Lankford coefficients R_0, R_{45} and R_{90} , the evolution of the uniaxial yield stress $\sigma(\alpha)$ can be strongly modified by changing the values of exponents m, n and p , while it is almost unaffected by the choice of other material parameters. This result will be turned to account to split the identification procedure in two steps, as proposed below.

The strain hardening parameters are first identified using the uniaxial tensile tests. Then, the following procedure is adopted to identify the material parameters of the yield function :

Parameters defining the yield surface :
 8 parameters : k, A, B, m, n, p, a, b

First step : analysis of uniaxial tensile tests :
Data : R_0, R_{45}, R_{90}
Procedure : take $k = 0$, determine the (m, n, p) values fitting the evolution of $\sigma(\alpha)$ (the parameters A, a and b are determined knowing R_0, R_{45} and R_{90})
 keep the (m, n, p) values for the continuation of identification.

Second step : analysis of heterogeneous biaxial tensile tests :
Data : R_0, R_{45}, R_{90} , experimental strain fields
Procedure : analyse the response surface of the cost function to determine the (k, B) pair minimizing the difference between experimental and calculated strain fields
 (for each (k, B) pair, A, a and b are re-calculated knowing R_0, R_{45} and R_{90})

4. IDENTIFICATION RESULTS

Three materials were tested, i.e.: an Interstitial Free (IF) steel, a commercial purity aluminum, which was annealed for 100 min. at 310°C, and an aluminum alloy of the type A 5086 H111.

The first step of the identification consists of analyzing the uniaxial tensile tests. For IF steel and aluminum, strain-hardening was described at best with the Swift law:

$$\bar{\sigma} = K(\varepsilon_0 + \bar{\varepsilon}^p)^N \tag{5}$$

where K , ε_0 and N are material constants. For type A 5086 aluminum alloy, the Voce law was used:

$$\bar{\sigma} = \sigma_s(1 - \alpha \exp(\beta \bar{\varepsilon}^{-p})) \tag{6}$$

where σ_s , α and β are material constants. The strain hardening parameters and the R -values are given in Table 1 and 2, respectively.

Table 1 Coefficients of the hardening laws

Swift law	K (MPa)	ε_0	N
IF steel	510	0.004	0.2366
Aluminum	149	0.004	0.2870
Voce law	σ_s (MPa)	α	β
A 5086 alloy	380	0.579	-10.35

Table 2 Lankford coefficients

	R_0	R_{45}	R_{90}
IF steel	2.30	1.74	2.87
Aluminum	0.80	0.55	0.89
A 5086 alloy	0.70	0.86	0.71

An illustration of the identification of (m, n, p) exponents is presented on fig. 4 for IF steel. The experimental values of σ_{45}/σ_0 and σ_{90}/σ_0 are represented with intervals corresponding to the values determined at different values of expended plastic work. The best fit for the evolution of $\sigma(\alpha)$ is obtained with $m=2$, $n=3$ and $p=2$. The results obtained with Hill’s criterion are also shown for comparison.

The (m, n, p) exponents identified for the 3 materials are given in Table 3.

Table 3 Values of the (m, n, p) exponents

	m	n	p
IF steel	2	3	2
Aluminum	2	1	3
A 5086 alloy	2	3	3

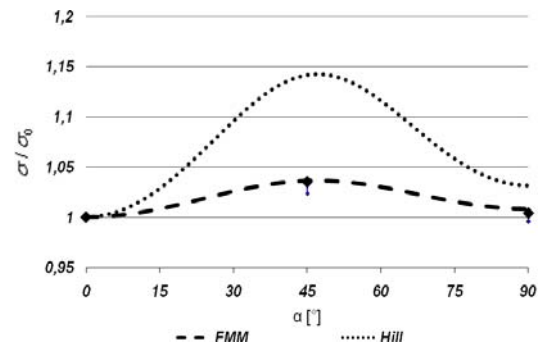


Fig. 4 Angular variation of the flow stress σ for IF steel

The second step of the identification procedure consists of running the finite element simulations by changing the (k, B) pair in order to minimize the cost function:

$$\Phi(P) = \frac{1}{n} \sum_{i=1}^n \left(\frac{\varepsilon_i(k, B) - \varepsilon_i^{\text{exp}}}{\varepsilon_i^{\text{exp}}} \right)^2 \tag{7}$$

where $\varepsilon_i(k, B)$ is the value of the major principal strain calculated at point i with the current (k, B) pair and $\varepsilon_i^{\text{exp}}$ is the experimental value at point i .

The strain fields used for the identification procedure are the major principal strains along, (a) the symmetry axes of UT/PST specimens corresponding to the RD and the TD, (b) the line inclined at 45° from the preceding axes (diagonal direction, DD), (c) the symmetry axes of UT/EBT specimens corresponding to the RD and the TD. To find the minimum of the cost function, the response surface was first analyzed over a wide (k, B) domain, next over a refined one.

An example of the best-fit curves obtained along the different lines is given in fig. 5 for IF steel. The strain distributions calculated with Hill’s criterion are also shown for comparison in order to display the high sensitivity of the identification method.

Finally, the material parameters (k, A, B, a, b) determined for the 3 materials are given in Table 4, and the plane stress yield surfaces obtained by the identification procedure are shown in fig. 6.

Table 4 Values of the (k, A, B, a, b) parameters

	k	A	B	a	b
IF steel	-1	4.43	5	-0.098	0.730
Aluminum	0.3	2.31	5	-0.074	0.509
A 5086 alloy	0.4	2.88	6	-0.005	-0.276

5. EARING IN CUP DRAWING

The cup drawing tests were performed with a specific device. The punch diameter is equal to 30 mm. The circular blanks have a diameter of 66 mm

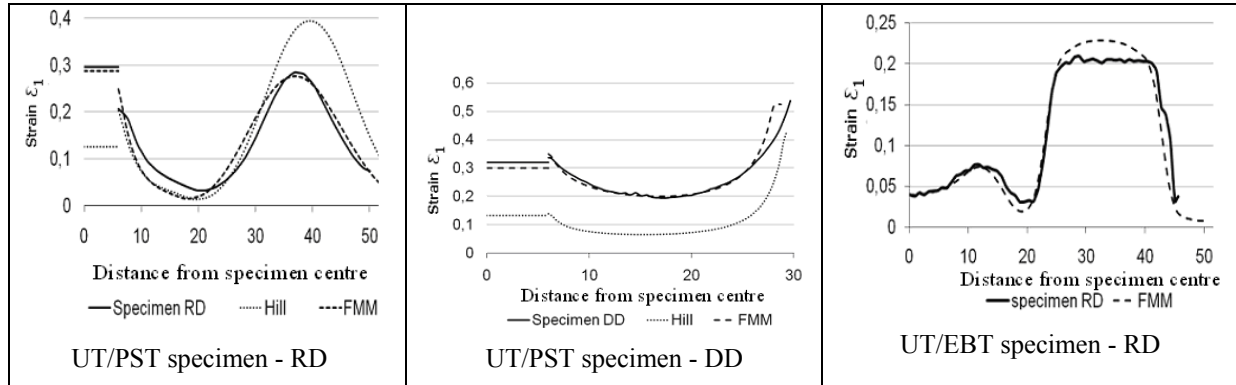


Fig. 5 Comparison between experimental and calculated strain distributions for IF steel

The horizontal lines for UT/PST specimen represent the deformation $Ln(r/r_0)$ of the central hole.

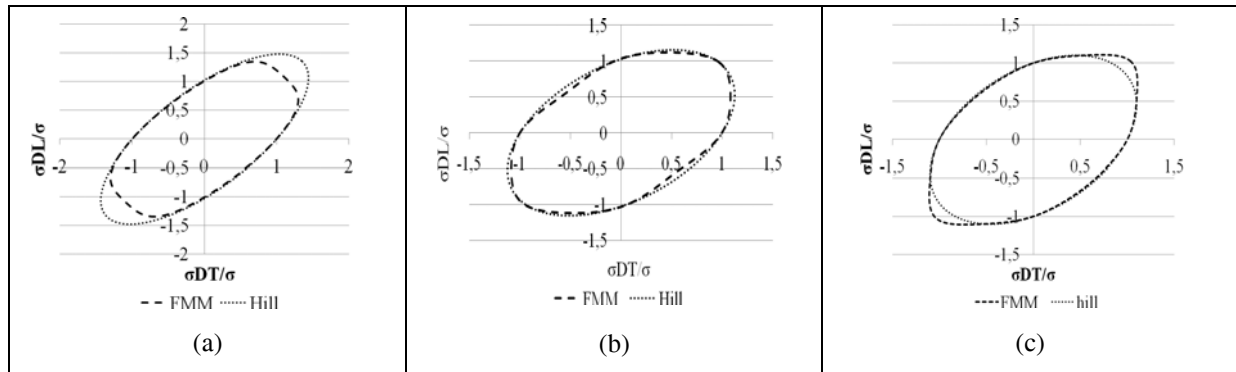


Fig. 6 Yield surfaces identified for (a) IF steel, (b) aluminum and (c) A 5086 alloy

for IF steel, 51 mm for aluminum and 57 mm for A 5086 alloy. The drawing ratio DR , defined by the ratio between blank diameter and punch diameter, is thus equal to 2.2, 1.7 and 1.9, respectively.

The numerical simulations of the drawing tests were performed using the material parameters obtained by the identification procedure (Tables 1-4). The comparison between experimental and predicted earing profiles is shown in fig. 7. It can be observed that the height of ears is well predicted.

For comparison, the height of ears obtained with Hill’s criterion is too large. This behavior should be put in correspondence with the unrealistically large variations of $\sigma(\alpha)$ predicted by Hill’s criterion, fig. 4. In agreement with the argument presented in section 1, an accurate description of stress anisotropy, i.e., of the angular variation of $\sigma(\alpha)$, thus is quite important for obtaining an accurate prediction of plastic flow and earing formation.

Following an earlier proposal by Zaky et al. 15], an attempt was made to modify the initial contour of the blank, in order to obtain ear-free cups. The shape of the modified contour is defined by the angular variation of the blank radius:

$$\rho(\alpha) = \rho_0 - \frac{1}{DR}(H(\alpha) - H_0) \tag{8}$$

where $\rho(\alpha)$ and ρ_0 are the blank radii at the current angle α and at $\alpha=0^\circ$ from RD, respectively, and $H(\alpha)$ and H_0 are the heights of ears obtained on circular contours at the current angle α and at $\alpha=0^\circ$ from RD, respectively.

The pictures of deep-drawn cups obtained on IF steel blanks with a circular contour and with a modified contour are shown in fig. 8. The modified contour was obtained by polishing the edge of an initially circular blank in order to satisfy equation 8. In comparison with the well-developed ears obtained on the circular contour, the angular variations of cup height are much less for the modified contour. However, we could not avoid slight irregularities on the edge of the deep-drawn cup, due to imperfections of the initial contour, in spite of the care taken to obtain this contour. Indeed, the simulations with the modified contour predict a quasi perfect ear-free cup.

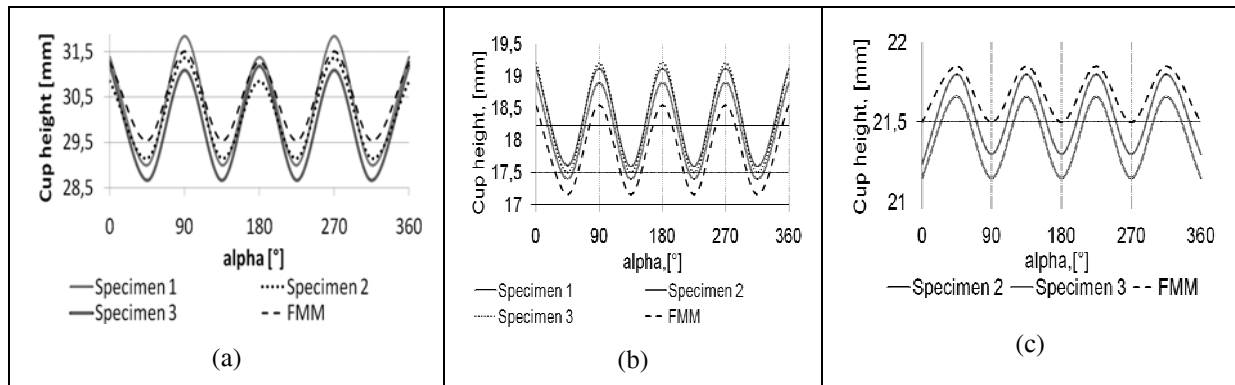


Fig. 7 Comparison between experimental and predicted earing profiles for circular blanks.
(a) IF steel, (b) aluminum, (c) A 5086 alloy

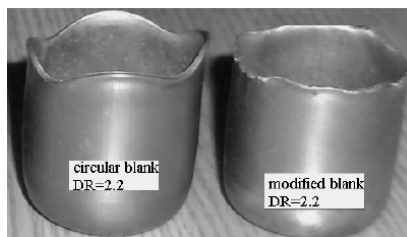


Fig. 8 Pictures of deep-drawn cups with initially circular and modified contours - IF steel

6. CONCLUSION

The identification of the anisotropic plastic behavior of metal sheets has been performed on three materials by combining the results of uniaxial tensile tests and heterogeneous biaxial tensile tests. The biaxial specimens have been designed in order to obtain a high sensitivity of strain fields to the material parameters describing the shape of the yield surface in the biaxial stretching range.

The identification procedure consists of two steps. In the first step, the uniaxial tensile tests are analyzed to determine the hardening law of the material, and the parameters of the yield function which allow us to obtain a good description of both *strain*-anisotropy (variation of the Lankford coefficient R in the plane of the sheet) and *stress*-anisotropy (variation of the uniaxial flow stress σ in the plane of the sheet). In the second step, an optimization procedure is used to minimize the difference between experimental strain fields obtained by an image correlation method, and numerically-predicted strain fields. The additional material parameters of the yield function are determined in this way. Based on this identification, the earing profile predicted on deep-drawn cups was compared with experimental ones. As a result of the good description of both *strain*-anisotropy and *stress*-anisotropy, very good predictions of ears are obtained in the numerical simulations. A modified contour of the blank also has been tested to obtain ear-free cups.

REFERENCES

- [1] Chung, K., Shah, K., *Finite element simulation of sheet metal forming for planar anisotropic metals*, International Journal of Plasticity, 8, 1992, pag. 453-476;
- [2] Moreira, L.P., Ferron, G., Ferran, G., *Experimental and numerical analysis of the cup drawing test for orthotropic metal sheets*, Journal of Materials Processing Technology, 108, 2000, pag. 78-86;
- [3] Moreira, L. P., Ferron, G., *Influence of the plasticity model in sheet metal forming simulations*, Journal of Materials Processing Technology, 155-156, 2004, pag. 1596-1603;
- [4] Bourne, L., Hill, R., *Philosophical Magazine*, 41, 1950, pag. 671;
- [5] Barlat, F., Panchanadeeswaran, S., Richmond, O., *Prediction of earing in cup drawing fcc materials*, Textures and Microstructures, 14-18, 1991, pag. 507-512;
- [6] Ferron, G., Makinde, A., *Design and development of a biaxial strength testing device*, Journal of Testing and Evaluation, 6(3), 1988, pag. 253-256;
- [7] Hill, R., *A theory of the yielding and plastic flow of anisotropic metals*, Proceedings of the Royal Society of London, A 193, 1948, pag. 281-297;
- [8] Barlat, F., Richmond, O., *Prediction of tricomponent plane stress yield surfaces and associated flow and failure behavior of strongly textured f.c.c. polycrystalline sheets*, Materials Science and Engineering, 95, 1987, pag. 15-29;
- [9] Barlat, F., Lege, D.J., Brem, J.C., *A six-component yield function for anisotropic materials*, International Journal of Plasticity, 7, 1991, pag. 693-712;
- [10] Karafillis, A.P., Boyce, M.C., *A general anisotropic yield criterion using bounds and a transformation weighting tensor*, Journal of the Mechanics and Physics of Solids, 41, 1993, pag. 1859-1886;
- [11] Ferron, G., Makkouk, R., Morreale, J., *A parametric description of orthotropic plasticity in metal sheets*, International Journal of Plasticity, 10, 1994, pag. 431-449;
- [12] Banabic, D., Aretz, H., Comsa, D.S., Paraianu, L., 2005. *An improved analytical description of orthotropy in metallic sheets*, International Journal of Plasticity, 21, 1987, pag. 493-512;
- [13] Barlat, F., Yoon, J.W., Cazacu, O., *On linear transformations of stress tensors for the description of plastic anisotropy*, International Journal of Plasticity, 23, 2007, pag. 876-896;
- [14] Moreira, L. P., Ferron, G., *Influence of the plasticity model in sheet metal forming simulations*, Journal of Materials Processing Technology, 155-156, 2004, pag. 1596-1603.
- [15] Zaky, A.M., Nassr, A.B., El-Sebaie, M.G., *Optimum blank shape of cylindrical cups in deep-drawing of anisotropic sheet metals*, Journal of Materials Processing Technology, 76, 1998